PAPER

Design and optimization of a bend-and-sweep compliant mechanism

Smart Mater. Struct. **22** (2013) 094019 (11pp) doi:10.1088/0964-1726/22/9/094019

Design and optimization of a bend-and-sweep compliant mechanism

Y Tummala[1], M I Frecker[1], A A Wissa[2] and J E Hubbard Jr[2]

[1] Department of Mechanical and Nuclear Engineering, The Pennsylvania State University, University Park, PA, USA
[2] Department of Aerospace Engineering, University of Maryland and The National Institute of Aerospace, Hampton, VA, USA

E-mail: yashwanth.tummala@gmail.com

Received 29 January 2013, in final form 3 June 2013
Published 27 August 2013
Online at stacks.iop.org/SMS/22/094019

Abstract
A novel contact aided compliant mechanism called bend-and-sweep compliant mechanism is presented in this paper. This mechanism has nonlinear stiffness properties in two orthogonal directions. An angled compliant joint (ACJ) is the fundamental element of this mechanism. Geometric parameters of ACJs determine the stiffness of the compliant mechanism. This paper presents the design and optimization of bend-and-sweep compliant mechanism. A multi-objective optimization problem was formulated for design optimization of the bend-and-sweep compliant mechanism. The objectives of the optimization problem were to maximize or minimize the bending and sweep displacements, depending on the situation, while minimizing the von Mises stress and mass of each mechanism. This optimization problem was solved using NSGA-II (a genetic algorithm). The results of this optimization for a single ACJ during upstroke and downstroke are presented in this paper. Results of two different loading conditions used during optimization of a single ACJ for upstroke are presented. Finally, optimization results comparing the performance of compliant mechanisms with one and two ACJs are also presented. It can be inferred from these results that the number of ACJs and the design of each ACJ determines the stiffness of the bend-and-sweep compliant mechanism. These mechanisms can be used in various applications. The goal of this research is to improve the performance of ornithopters by passively morphing their wings. In order to achieve a bio-inspired wing gait called continuous vortex gait, the wings of the ornithopter need to bend, and sweep simultaneously. This can be achieved by inserting the bend-and-sweep compliant mechanism into the leading edge wing spar of the ornithopters.

(Some figures may appear in colour only in the online journal)

Nomenclature

α	Parameter to determine cutoff stress in the optimization
λ	Binary variable
ρ_{delrin}	Density of Delrin$^{\text{TM}}$ (kg m^{-3})
ϕ	Contact angle of the ACJ (deg)
ϕ_{cj}	Compliant joint angle of the ACJ (deg)
ϕ_k	Contact angle of the kth ACJ (deg)
$\phi_{k\text{cj}}$	Compliant joint angle of the kth ACJ (deg)
σ_{cutoff}	Stress limit on BSCM designs used during BSCM optimization (Pa)
$\sigma_{\max}$	Maximum von Mises stress in a BSCM (Pa)
σ_{penalty}	Penalty value for stress objective function (Pa)
σ_{yield}	Yield stress of BSCM material (Pa)
e	Eccentricity of the compliant hinge (m)
e_k	Eccentricity of the kth compliant hinge
f_1	Mass objective function in BSCM optimization
f_2	Bending deflection objective function in BSCM optimization
f_3	Stress objective function in BSCM optimization
f_4	Sweep deflection objective function in BSCM optimization
g_c	Contact gap between the contact surfaces (m)

k	Variable used to represent an ACJ's number
lb_{ϕ}	Lower bound on the contact angle of an ACJ
$\text{lb}_{\phi\text{cj}}$	Lower bound on the compliant joint angle of an ACJ
lb_{e}	Lower bound on the eccentricity of a CH
lb_{in}	Lower bound on the inner radius of a CH
lb_{out}	Lower bound on the outer radius of a CH
ub_{ϕ}	Upper bound on the contact angle of an ACJ
$\text{ub}_{\phi\text{cj}}$	Upper bound on the compliant joint angle of an ACJ
ub_{e}	Upper bound on the eccentricity of a CH
ub_{in}	Upper bound on the inner radius of a CH
ub_{out}	Upper bound on the outer radius of a CH
M	Mass of a BSCM (kg)
M_{penalty}	Penalty value for mass objective function (kg)
R_{in}	Inner radius of a single compliant hinge (m)
$R_{k\ \text{in}}$	Inner radius of the kth compliant hinge
$R_{k\ \text{out}}$	Outer radius of the kth compliant hinge
R_{out}	Outer radius of a single compliant hinge (m)
T	Maximum number of ACJs in a BSCM
X	Sweep direction
X_{max}	Sweep tip deflection observed in a BSCM (m)
X_{penalty}	Penalty value used for sweep deflection objective function (m)
Y	Direction along the length
Z	Bending direction
Z_{penalty}	Penalty value used for bending deflection objective function (m)
Z_{max}	Bending tip deflection observed in a BSCM (m)

1. Introduction

Contact aided compliant mechanisms (CCMs) are a class of compliant mechanisms where the compliant members come into contact with one another to perform a specific task or to improve the performance of the mechanism itself. A wide variety of contact interactions, which can range from a simple case involving single point contact to the more complex case of multiple contacts between different parts of the compliant mechanism itself, can be used to perform special tasks. These mechanisms were first introduced in the literature by Mankame and Ananthasuresh in 2002 [1]. Such mechanisms can have nonlinear stiffness [2–4], stress relief capabilities [5, 6] and can also generate a non-smooth path [1]. Mankame and Ananthasuresh have presented a displacement delimited contact aided compliant gripper [1]. They have also presented a CCM which uses intermittent contacts to convert reciprocating translation into two output curves to enclose a two-dimensional region [7]. Other CCMs that trace prescribed, non-smooth paths in response to a single, monotonically increasing input force were also synthesized by the same authors using topology optimization [8]. Reddy *et al* designed CCMs to trace large, non-smooth paths using topology optimization and finite element analysis (FEA) [9]. Mehta *et al* have designed honeycomb cells with contact elements called contact aided cellular compliant mechanisms (C^3Ms) to obtain stress relief [10]. Cirone *et al* have designed these C^3Ms with curved walls for high strain applications [11]. Halverson *et al* have designed a bi-axial CCM for spinal arthroplasty [12]. Cannon and Howell have designed a contact aided compliant revolute joint [13].

The bend-and-sweep compliant mechanism presented in this paper is also a contact aided compliant mechanism. This mechanism is designed to have nonlinear stiffness properties in two orthogonal directions. A contact aided compliant mechanism with bidirectional nonlinear stiffness has not been reported previously in the literature. The design of compliant mechanisms with desired stiffness properties in orthogonal directions has been considered by some researchers. Bubert *et al* have designed a morphing skin using a zero-Poisson honeycomb structure which can achieve 100% in-plane, uniaxial extension but is very stiff in the out-of-plane direction [14]. Vocke *et al* tested this mechanism in a wind tunnel [15]. Barbarino *et al* have designed a morphing cellular structure which is flexible in the in-plane direction but is stiff in the out-of-plane direction [16]. This mechanism was designed to achieve chord morphing of helicopter rotor blades.

The bend-and-sweep compliant mechanism presented in this paper is designed to enable passive shape change in an avian-scale ornithopter. Ornithopters, or flapping wing unmanned aerial vehicles (UAVs), have the potential to revolutionize UAV performance in both the civil and military sectors [17]. This work aims at improving the performance of these ornithopters during steady level flight by integrating passive compliant mechanisms into the wing structure. Previous work by the authors has shown that such an approach is feasible and that implementation of a one degree of freedom (DOF) compliant mechanism resulted in significant improvements in the performance of a test ornithopter [4, 18]. To achieve an avian-inspired wing gait in the ornithopter, the outer section of the wing must bend and sweep simultaneously during the upstroke, while remaining fully extended during the downstroke, as seen in birds (figure 1(a)) [18]. Bending of the ornithopter's wings is in the Z-direction, sweep is in the X-direction and twisting of the wings (represented by Ψ) is about the Y-axis as shown in figure 1(b). The bend-and-sweep compliant mechanism is primarily designed to cause simultaneous *passive* bending and sweep of the ornithopter's wings. It is possible that some twisting could occur as well. Very few researchers have considered passive approaches to shape change of flapping wing UAVs. One approach implemented a single, traditional torsional spring at the wrist location [19]. The torsional spring design was able to achieve passive bending during flapping, but resulted in severe thrust penalties. Hence a more sophisticated compliant joint was necessary. This led to the design of a compliant spine for passive bending during flight, which was successfully fabricated and tested by the authors [4]. Traditional mechanisms will not be able to achieve bidirectional stiffness in two orthogonal directions. Finally, weight added to the ornithopter due to these mechanisms will have to be minimal. Hence a compliant mechanism without pin joints is necessary for the desired application. To design these compliant mechanisms for passive shape change, this paper presents a new

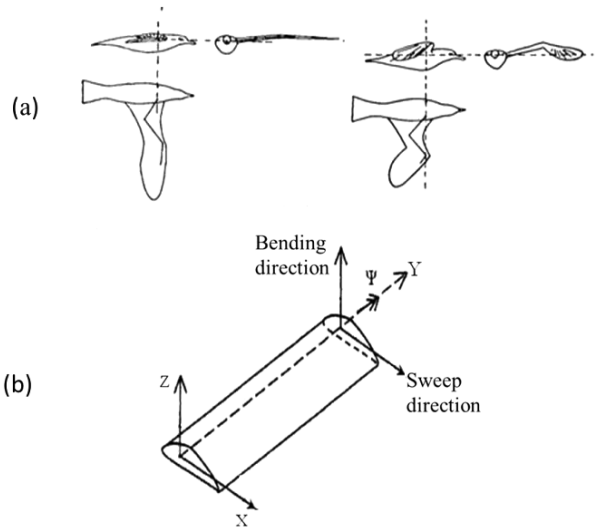

Figure 1. (a) Wings are fully extended at mid-downstroke (left). Wings are bent, twisted, and swept at mid-upstroke (right). Adapted with permission from [20]. (b) Bending, sweep and twist directions shown on an aircraft's right wing. Adapted with permission from [21].

design optimization procedure using nonlinear finite element analysis and genetic algorithms. The nonlinear finite element analysis includes nonlinear material properties and contact. This procedure will present the designer with performance tradeoffs which can be used to choose a suitable design for a specific application.

The remainder of this paper is organized as follows. Section 2 introduces the bend-and-sweep compliant mechanism design and its fundamental element. Section 3 presents the concomitant design optimization problem that was formulated to design bend-and-sweep compliant mechanisms for the ornithopter application. Design optimization results are presented as a case study in section 4. Finally, conclusions are drawn and future work is discussed in section 5.

2. Bend-and-sweep compliant mechanism

The bend-and-sweep compliant mechanism (BSCM) is a novel contact aided compliant mechanism with nonlinear stiffness properties. This compliant mechanism has two orthogonal degrees of freedom, one that will allow in-plane bending and another that will allow out-of-plane bending (also called sweep). A bend-and-sweep compliant mechanism with three angled compliant joints (ACJs) is shown in figure 2. The angled compliant joint is the fundamental element of this mechanism (shown in figure 3). The semi-circular hinge shown in figure 2 is called a compliant hinge. Each ACJ has a compliant hinge (CH). In this figure, and for the remainder of this paper, Z-direction denotes the bending direction while X-direction denotes the sweep direction. The nonlinear stiffness of a BSCM can be tailored by changing the geometry of an ACJ and also by changing the number of ACJs.

A BSCM is flexible when it is deformed in the negative Z-direction because of the compliant hinge. Because this

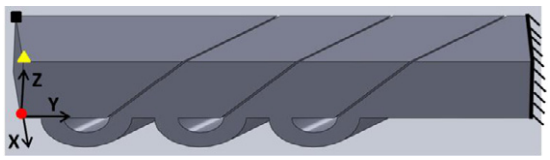

Figure 2. Bend-and-sweep compliant mechanism. This mechanism has three angled compliant joints.

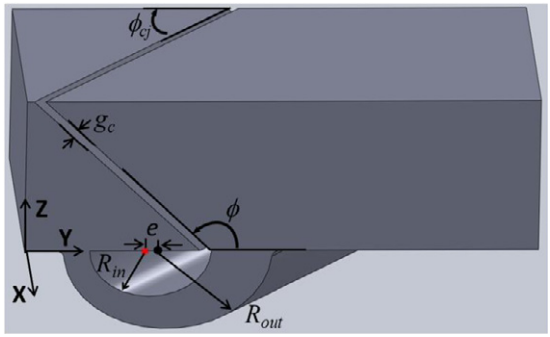

Figure 3. Fundamental element of the BSCM mechanism, called an ACJ. The geometric parameters that affect the stiffness of this mechanism are shown in the figure.

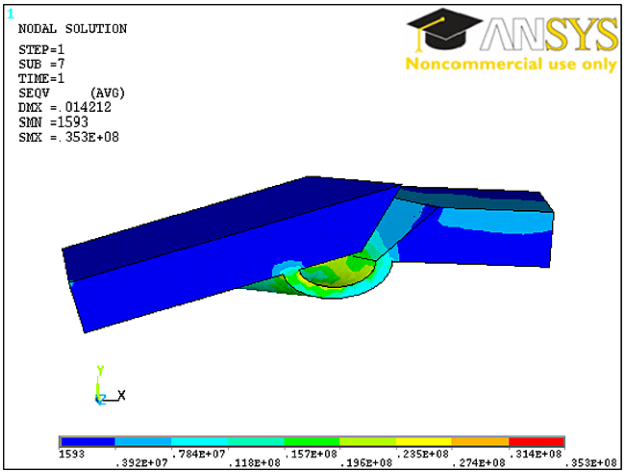

Figure 4. Deformed BSCM in the $-X$-direction and $-Z$-direction. The BSCM is very flexible in the $-X$ and $-Z$ directions.

hinge is compliant, large deformations can occur (figure 4). On the other hand, this mechanism is very stiff when it is deformed in the positive Z-direction because of the angled contact surfaces (figure 5). During such deformations these contact surfaces come into contact, making the mechanism stiff. Thus the mechanism has nonlinear stiffness properties. A stiffness plot illustrating the nonlinear stiffness of a sample design is shown in figure 6. This stiffness plot was generated using a BSCM with one ACJ (shown in figures 4 and 5). The right face of the BSCM was fixed (as shown in figure 2) and equal tip loads were applied in the X- and Z-directions. Locations where these tip loads were applied on a BSCM are shown by a black square, yellow triangle and a red circle. Bending tip loads were applied at the black square and yellow

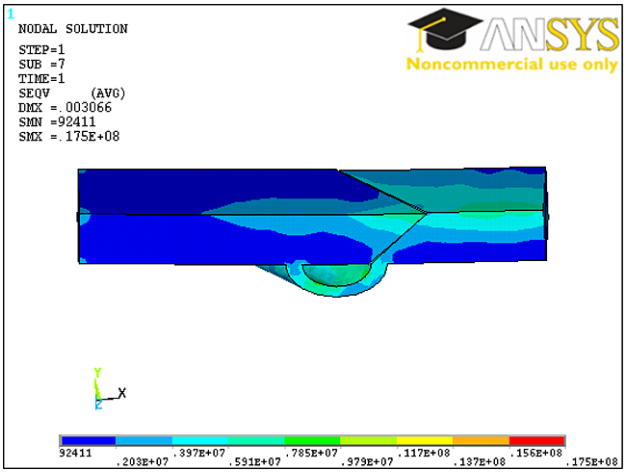

Figure 5. Deformed BSCM in the $+X$-direction and $+Z$-direction. The BSCM is very stiff in the $+X$ and $+Z$ directions.

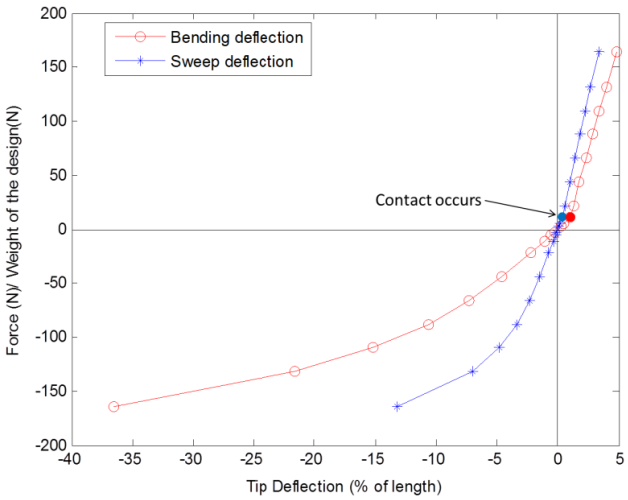

Figure 6. Stiffness plot illustrating nonlinear stiffness of a sample BSCM. After contact, the stiffness of the BSCM increases significantly.

triangle while sweep tip loads were applied at the yellow triangle and red circle.

As shown in figure 3, the geometric parameters that affect the stiffness of this mechanism are the inner (R_{in}) and outer radii (R_{out}) of the compliant hinge, contact angle (ϕ), compliant joint angle (ϕ_{cj}), contact gap between the contact surfaces (g_{c}), and eccentricity of the compliant hinge (e). The black dot in the figure represents the center of the outer semi-circle and the red star represents the center of the inner semi-circle of the compliant hinge. The value of the parameter e is positive if the black dot is to the right of the red star and is negative if it is otherwise; except when the black dot and red star coincide, when it has a value of zero. The contact gap (g_{c}) of a compliant joint is the perpendicular distance between the slanted contact surfaces.

A design optimization methodology was developed to design these mechanisms for the ornithopter application. This design optimization procedure can be used to design contact aided compliant mechanisms using nonlinear finite element analysis and genetic algorithms for shape morphing. Nonlinear finite element analysis includes nonlinear material properties and contact. This procedure presents the designer with tradeoffs. Such results can be used to choose a good design for any specific application. This design optimization methodology is presented in section 3.

3. Design optimization

There are six geometric parameters that define the stiffness of an ACJ (see figure 3). Among these parameters, contact gap (g_{c}) is fixed. To determine the best values of all other geometric parameters and also the number of ACJs in a BSCM, multi-objective optimization problems are formulated. The optimization problem that was defined for upstroke to maximize the magnitudes of bending and sweep deflections is given by equations (1)–(11). The optimization problem that was defined for downstroke to minimize the magnitudes of both bending and sweep deflections is given by equations (12)–(22). These optimization problems are solved using a genetic algorithm.

Multi-objective optimization problem to maximize the magnitudes of bending and sweep deflections for upstroke:

$$\begin{aligned} &\text{minimize } (f_1, f_3) \\ &\text{maximize } (f_2, f_4) \end{aligned}$$

subject to

$$\begin{aligned} R_{k\text{ in}} - R_{k\text{ out}} + |e_k| &\leq 0 \\ \text{lb}_{\text{in}} \leq R_{k\text{ in}} &\leq \text{ub}_{\text{in}} \\ \text{lb}_{\text{out}} \leq R_{k\text{ out}} &\leq \text{ub}_{\text{out}} \\ \text{lb}_{\text{e}} \leq e_k &\leq \text{ub}_{\text{e}} \\ \text{lb}_{\phi} \leq \phi_k &\leq \text{ub}_{\phi} \\ \text{lb}_{\phi_{\text{cj}}} \leq \phi_{kcj} &\leq \text{ub}_{\phi_{\text{cj}}} \\ k = 1, 2, 3, \ldots, T & \end{aligned} \tag{1}$$

where

$$f_1 = \lambda M + (1-\lambda) M_{\text{penalty}} \tag{2}$$

$$f_2 = |\lambda Z_{\max} - (1-\lambda) Z_{\text{penalty}}| \tag{3}$$

$$f_3 = \lambda \sigma_{\max} + (1-\lambda) \sigma_{\text{penalty}} \tag{4}$$

$$f_4 = |\lambda X_{\max} - (1-\lambda) X_{\text{penalty}}| \tag{5}$$

$$\lambda = \begin{cases} 1 & \text{if } \sigma_{\max} \leq \sigma_{\text{cutoff}} \\ 0 & \text{if } \sigma_{\max} > \sigma_{\text{cutoff}} \end{cases} \tag{6}$$

$$\sigma_{\text{cutoff}} = \alpha \sigma_{\text{yield}} \tag{7}$$

$$M_{\text{penalty}} \gg M \tag{8}$$

$$Z_{\text{penalty}} \ll Z_{\max} \tag{9}$$

$$\sigma_{\text{penalty}} \gg \sigma_{\max} \tag{10}$$

$$X_{\text{penalty}} \ll X_{\max}. \tag{11}$$

Multi-objective optimization problem to minimize the magnitudes of bending and sweep deflection for downstroke:

$$\text{minimize } (f_1, f_2, f_3, f_4)$$

subject to

$$\begin{aligned} R_{k\,\text{in}} - R_{k\,\text{out}} + |e_k| &\leq 0 \\ \text{lb}_{\text{in}} \leq R_{k\,\text{in}} &\leq \text{ub}_{\text{in}} \\ \text{lb}_{\text{out}} \leq R_{k\,\text{out}} &\leq \text{ub}_{\text{out}} \\ \text{lb}_{\text{e}} \leq e_k &\leq \text{ub}_{\text{e}} \\ \text{lb}_{\phi} \leq \phi_k &\leq \text{ub}_{\phi} \\ \text{lb}_{\phi_{\text{cj}}} \leq \phi_{kcj} &\leq \text{ub}_{\phi_{\text{cj}}} \\ k = 1, 2, 3, \ldots, T & \end{aligned} \tag{12}$$

where

$$f_1 = \lambda M + (1-\lambda) M_{\text{penalty}} \tag{13}$$

$$f_2 = |\lambda Z_{\max} - (1-\lambda) Z_{\text{penalty}}| \tag{14}$$

$$f_3 = \lambda \sigma_{\max} + (1-\lambda) \sigma_{\text{penalty}} \tag{15}$$

$$f_4 = |\lambda X_{\max} - (1-\lambda) X_{\text{penalty}}| \tag{16}$$

$$\lambda = \begin{cases} 1 & \text{if } \sigma_{\max} \leq \sigma_{\text{cutoff}} \\ 0 & \text{if } \sigma_{\max} > \sigma_{\text{cutoff}} \end{cases} \tag{17}$$

$$\sigma_{\text{cutoff}} = \alpha \sigma_{\text{yield}} \tag{18}$$

$$M_{\text{penalty}} \gg M \tag{19}$$

$$Z_{\text{penalty}} \gg Z_{\max} \tag{20}$$

$$\sigma_{\text{penalty}} \gg \sigma_{\max} \tag{21}$$

$$X_{\text{penalty}} \gg X_{\max}. \tag{22}$$

Geometric constraints on the design variables, given by equation (1), ensure that the inner and outer semi-circles of the hinges never intersect, thus creating feasible compliant hinges for all the BSCM designs. The objective functions f_1, f_2, f_3, and f_4 given by equations (2)–(5), respectively, are calculated using a commercial finite element package, ANSYS. Objective function f_1 is the mass, f_2 is the bending deflection, f_3 is the maximum von Mises stress and f_4 is the sweep deflection of a BSCM.

Constraints on the objective functions were imposed using the penalty values, M_{penalty}, Z_{penalty}, σ_{penalty}, X_{penalty}, and the binary variable λ. Penalty values (equations (8)–(11)) were chosen such that an infeasible design, determined by equation (6), was assigned a poor value of the objective function; such designs are terminated and not allowed to propagate into future generations. Such penalty values are chosen by the authors based on experience and it is suggested that they be at least five orders of magnitude higher than the objective functions. The optimization problem was solved using a genetic algorithm, NSGA-II. The objectives in this algorithm are always minimized. During optimization for upstroke, since the bending and sweep deflections are negative and their magnitudes need to maximized, the penalty terms are large positive numbers. During downstroke, since the absolute values of the deflections are being minimized, the penalty terms are still large positive numbers. Computational time is also an important factor in this optimization because finite element analysis is being performed on each of the BSCM designs in each generation. Taking the computational resources and complexity of the problem into consideration, penalty values have proved to be very effective in driving the optimization toward feasible regions in the design space. A BSCM design is considered to be infeasible if the maximum von Mises stress in the design, $\sigma_{\max}$, is greater than a cutoff stress limit, σ_{cutoff}, calculated from equation (7). This limit is controlled by the designer by choosing an appropriate value for α, which can be a function of the safety factor for a material with yield stress, σ_{yield}.

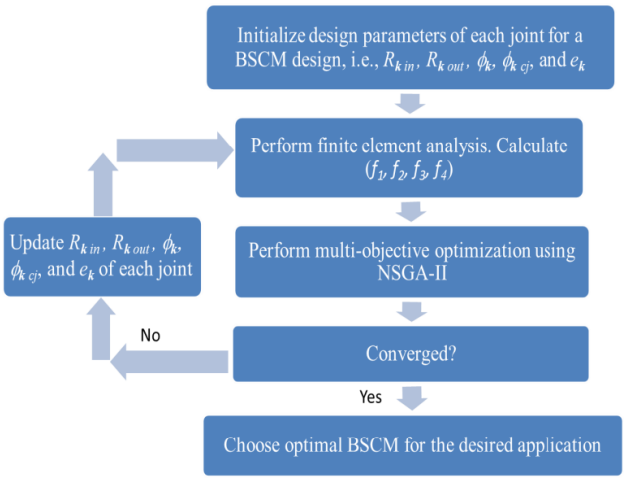

Figure 7. Schematic representation of the design optimization procedure for BSCM design. This procedure has been used to design BSCMs for ornithopter application.

An effective approach to solving the optimization problem is to use heuristic optimization algorithms such as multi-objective evolutionary algorithms (MOEAs). Zhou *et al* [22] present a survey of the state of the art MOEAs. A controlled elitist genetic algorithm which is a variant of NSGA-II [23, 24] was used for the optimization. This genetic algorithm is part of the optimization toolbox provided in MATLAB.

The optimization problem was implemented in an algorithm shown in the schematic in figure 7. The algorithm was stopped when convergence is achieved. Convergence of a multi-objective optimization problem can be determined with the help of various convergence metrics such as the convergence metric proposed by Deb and Jain [25]. Deb's metric is widely used in the field of MOEAs to test convergence. Kollat and Reed [26] use the same metric to compare the performance of different MOEAs. This metric, as was shown in [25], is a measure of the average distance between the reference set and the non-dominated population members of each of the generations; this average distance is normalized to always lie between 0 and 1. The optimization algorithm shown in figure 7 is said to have converged when the actual average distance is less than 0.08.

This design optimization methodology was implemented to design BSCMs that are to be used in an ornithopter application. Details of the application and the results of the optimization are presented as a case study in section 4.

4. Case study

One goal of this work is to improve the aerodynamic performance of ornithopters during steady level flight using

passive compliant mechanisms. This goal can be achieved by implementing the continuous vortex gait (CVG), a bio-inspired flight gait [27]. A more detailed description of the application of compliant mechanisms to achieve CVG in an ornithopter can be found in [4]. To implement CVG, the wings have to bend and sweep simultaneously during upstroke while remaining fully extended during downstroke. This can be achieved by inserting a BSCM in the leading edge spar of the ornithopter. Since BSCMs are passive in nature, they deform as a natural consequence to the aerodynamic loads acting on the ornithopter during flight. Hence, they are designed to provide the desired bend and sweep of the wings as a result of the lift and drag forces experienced by the ornithopter during steady level flight.

Bending of the wings is achieved because of the lift forces while sweep is mainly due to the drag forces. Unlike the lift forces, which change their direction during a single flapping cycle, the drag forces always act in one direction. During upstroke, the mechanism bends and sweeps in the $-Z$ and $-X$ directions, respectively. On the other hand the mechanism bends and sweeps in the $+Z$ and $-X$ directions, respectively, during downstroke. The goal of the optimization problem is to maximize the magnitude of deflection in both $-X$ and $-Z$ directions during upstroke, subject to stress constraints. Since bending and sweep are in $-X$ and $-Z$ directions, their results are shown as negative values in the plots. During downstroke, the objective is to minimize the magnitudes of both bending and sweep deflections. The bending deflection is positive while the sweep deflection is negative during downstroke because of the loading conditions. Results of both these optimization problems are presented here. To predict the deflections of the bend-and-sweep compliant mechanisms during the upstroke and downstroke, an estimate of the aerodynamic loads acting on the wing structure is needed.

To estimate the aerodynamic loads acting on the ornithopter wing structure, strain gage experiments were conducted by the authors and presented in [18]. The test ornithopter has a wing span of 1.06 m. Based on these results it was estimated that the maximum magnitude of the integrated lift loads during a flapping cycle at 5 Hz was 10 N [3]. During bench top testing of the ornithopter, it was found that the ornithopter generates a peak thrust of 3.12 N (0.7 lbf) at a flapping frequency of 5 Hz and zero forward velocity [18]. This means that each wing generates a thrust of 1.56 N (0.35 lbf). The ornithopter is capable of forward flight at a flapping frequency of 5 Hz. This implies that the thrust forces produced by the ornithopter at this frequency can overcome the drag forces. Hence we assume that the maximum drag force is 1.56 N.

Equivalent moments caused by these loads at the tip of the BSCM were used in the finite element analysis to design a BSCM for an ornithopter application. Two sets of loads were applied as pure moments acting on the BSCMs to simulate both upstroke and downstroke conditions during the optimization. During the upstroke, lift forces cause a positive bending moment about the X-axis while drag forces cause a negative moment about the Z-axis (figure 8). During the downstroke, lift forces cause a negative moment about the X-axis while the drag forces still cause the same negative moment about the Z-axis (figure 8).

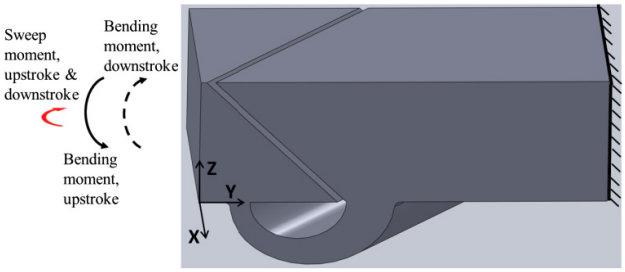

Figure 8. Loading conditions used during upstroke and downstroke simulations. Bending loads on the mechanism change direction between upstroke and downstroke while sweep loads do not.

Table 1. Different cases that were considered during design optimization of the BSCM.

Type of simulation	Upstroke/downstroke	T (number of ACJs)
Dynamic	Upstroke	1
Dynamic	Upstroke	2
Quasi-static	Upstroke	1
Quasi-static	Downstroke	1

The ornithopter application imposes dimensional constraints on the BSCM designs as it is based on an actual test platform [18]. The BSCM design was constrained to not be more than 63.5 mm long, 12.7 mm wide and 12.7 mm thick. These dimensional constraints limit the number of ACJs that can be accommodated in a single BSCM. As a case study, BSCMs with one and two ACJs were optimized using the design optimization procedure and the results are presented here.

Since the application is dynamic in nature, dynamic finite element analysis was performed on the BSCMs during optimization but the finite element package, ANSYS, could only perform linear analysis in this case. In reality, since, BSCMs are going to be fabricated out of Delrin^{TM} (Dupont polymer), large deformations, nonlinear material properties and contact must be incorporated in the finite element analysis. Hence an optimization using quasi-static analysis, which can account for large deformation, nonlinear material properties and contact, was also performed. All these cases are summarized in table 1. During the finite element analysis, Solid45, Conta174, Targe170, finite elements, large displacement quasi-static analysis, and multi-linear material properties of Delrin^{TM} were used [28, 29]. The frequency used in the *steady state* dynamic FEA corresponds to the flapping frequency, 5 Hz.

The upper and lower bounds used on the geometric parameters during optimization are shown in table 2. Based on the previous study [2], the best contact gap (g_c) was determined to be as small as possible, defined by the manufacturing process. Hence, it was fixed to be 0.3 mm. Other parameters that were used during the optimization are listed in table 3. The results of the design optimization of BSCMs are presented in section 4.1.

Table 2. Upper and lower bounds used on the geometric parameters during design optimization of the BSCM.

Design parameters	R_{in} (m)	R_{out} (m)	e (m)	ϕ (deg)	ϕ_{cj} (deg)
Lower bound	0.0004	0.0004	−0.004	20	20
Upper bound	0.006	0.006	0.004	160	160

Table 3. Other parameters that were used during the design optimization.

Variable	Value
α	1
σ_{yield}	45×10^6 Pa
$M_{penalty}$	13.4×10^6 kg
$Z_{penalty}$	1000 m
$X_{penalty}$	1000 m
$\sigma_{penalty}$	$10\,000 \times 10^6$ Pa
Population size	100
ρ_{delrin}	1420 kg m^{-3}
M_{max}	0.0145 kg

4.1. Optimization results

The optimization problem presented in the previous section had four objectives. Since it is a multi-objective optimization problem, the optimal solution is a set of points which are part of a Pareto front. A Pareto front is a set of optimal solutions that are not strictly dominated by any other designs of the design space. In other words, members of the Pareto front are among the best performing designs of the design space. A Pareto front member will not perform better than any other member with respect to a particular objective function without sacrificing performance in another objective function. The Pareto frontier in this optimization problem is 4D in nature, because there are four objective functions, and compares bending deflection, sweep deflection, mass and maximum von Mises stress simultaneously. A designer can analyze these Pareto fronts to understand the effect of geometric parameters on the performance metrics. For example, as the compliant joint angle becomes obtuse, the mass of the BSCM increases. Such trends can be observed from the Pareto plots. A population size of 100 was used for all the optimization procedures.

Advancement of the Pareto font of a two ACJ dynamic optimization for upstroke is shown in figure 9. The red squares represent members of the tenth generation while blue stars represent members of the 145th generation. The Pareto frontier moves toward the lower left corner of the plot, indicating that the magnitude of the bending deflection is being maximized while the stress is being minimized. This demonstrates the efficacy of the genetic algorithm. The red squares near the upper left corner represent infeasible designs in the design space. It can be seen from this plot that these infeasible designs are terminated in the later generations. Members of earlier generations are also less spread out.

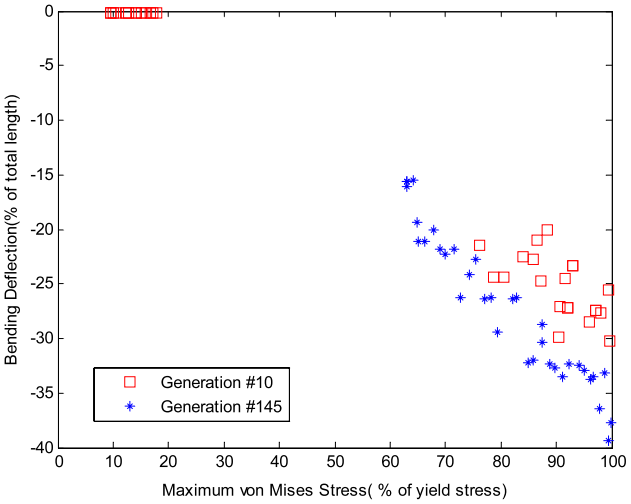

Figure 9. Advancement of the Pareto front of a two ACJ optimization for upstroke from the tenth generation to the 145th generation shows that the objectives are being minimized. Members of the earlier generations include infeasible designs and are less spread out.

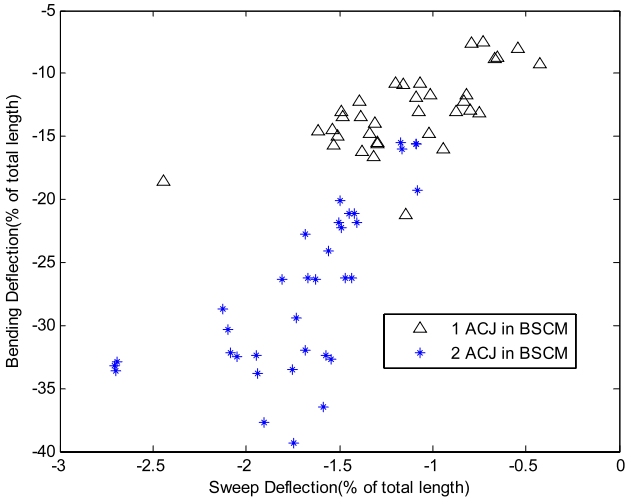

Figure 10. Pareto fronts of BSCMs with one and two ACJs comparing bending and sweep deflections. BSCMs with two ACJs generally have greater bending and sweep deflections than the ones with one ACJ.

Figures 10–12 show the Pareto plots of BSCMs with one and two ACJs. Since there are four objectives, comparing two objectives at a time will give six plots, of which only three are shown here for brevity. The three plots not shown are very similar to the three plots shown. Figures 13–16 show the Pareto fronts of the four cases presented in table 1. In all of these plots, the Y-axis represents the bending deflection, while the X-axis represents the sweep deflection. The size of the markers in these plots is a measure of relative mass of each of the designs. The color of the marker represents the maximum von Mises stress observed as a percentage of the yield stress of Delrin. Maximum von Mises stress is obtained from finite element analysis.

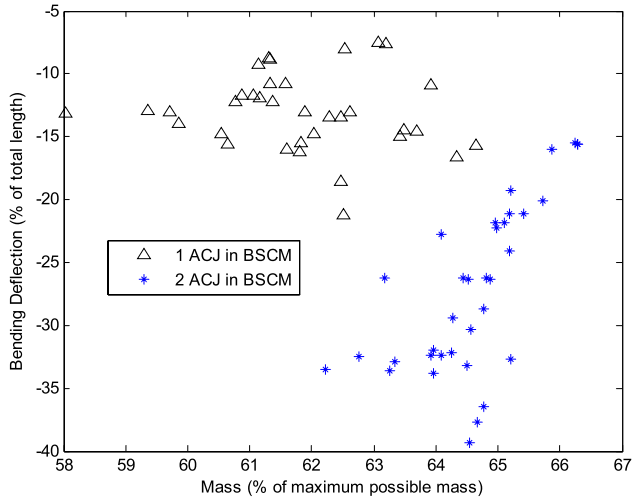

Figure 11. Pareto fronts of BSCMs with one and two ACJs comparing bending deflection and mass of the designs. BSCMs with two ACJs have more mass than the ones with one ACJ.

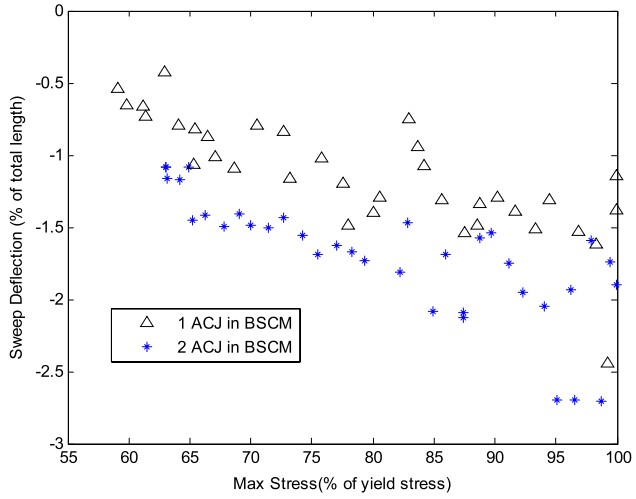

Figure 12. Pareto fronts of BSCMs with one and two ACJs comparing sweep deflection and maximum von Mises stress. For a particular von Mises stress value, the BSCMs with two compliant joints exhibit more bending and sweep deflections than those with one ACJ.

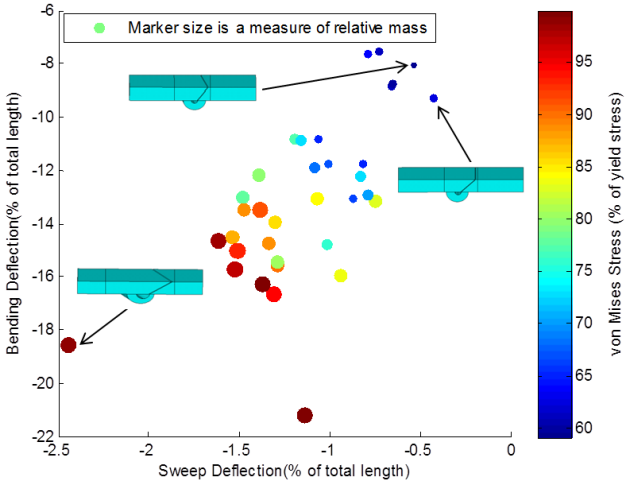

Figure 13. Pareto front of BSCM optimization with one ACJ during upstroke using dynamic analysis. As the compliant joint angle becomes obtuse the sweep and bending deflection of the BSCM increases.

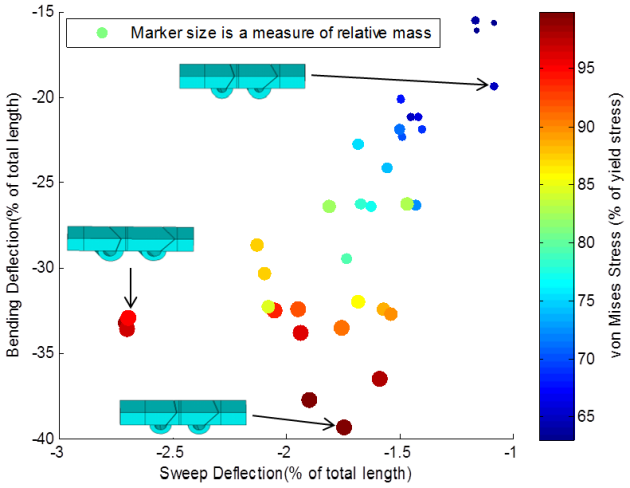

Figure 14. Pareto front of BSCM optimization with two ACJs during upstroke using dynamic analysis. As the deflections increase, stresses in the designs increase.

4.2. Discussion

Figures 10–12 compare the Pareto fronts of BSCMs with one and two ACJs. The blue dots, which represent BSCMs with two ACJs in figure 10, generally have greater bending and sweep deflections than the ones with one ACJ. Hence, it can be concluded that as the number of ACJs in a BSCM increase, the stiffness of the mechanism decreases. But such an increase in the number of ACJs also increases the mass of the BSCMs, which is evident from figure 11. Finally, figure 12 suggests that for a particular von Mises stress value, the BSCMs with two compliant joints exhibit greater bending and sweep deflections than those with one compliant joint. For the ornithopter application, and based on the desired bending and sweep deflections, the best number of ACJs in a BSCM can be determined.

Figure 13 shows the Pareto front of the BSCMs with one ACJ using dynamic analysis. This optimization converged after 190 generations. Three optimal BSCMs are highlighted in this plot as examples. A BSCM design pictured on the right in this figure has a compliant joint angle of 90°, resulting in the least possible sweep deflection. It should be observed that as the compliant joint angle becomes obtuse the sweep and bending deflections of the BSCM increase. This is confirmed by the BSCM designs shown. But such an increase in the compliant joint angle is accompanied by increases in mass and maximum von Mises stress in the BSCM designs. Also note that the maximum von Mises stress in the designs increases from the top right to the bottom left corner of the plot. This is because these designs have higher bending and sweep deflections; i.e., the larger the deflections, the larger are the stresses observed.

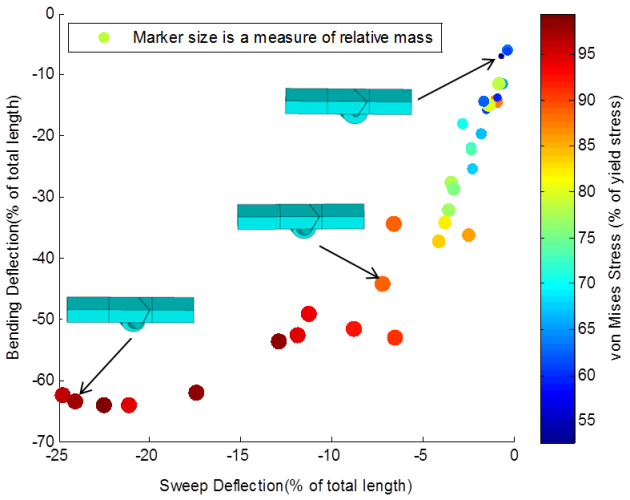

Figure 15. Pareto front of BSCM optimization with one ACJ during upstroke using quasi-static analysis. Quasi-static analysis takes large deformations into account.

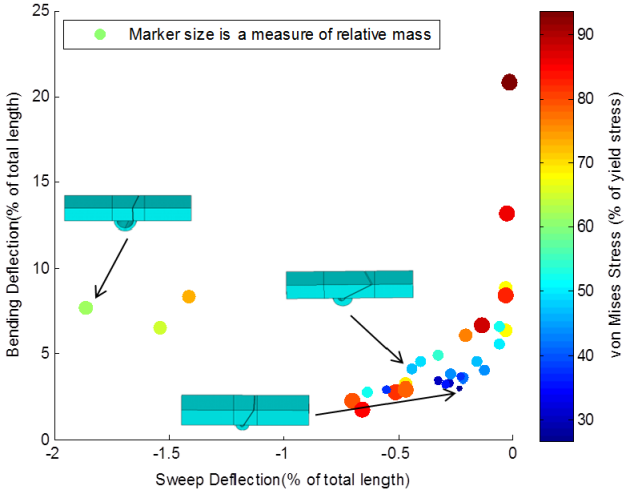

Figure 16. Pareto front of BSCM optimization with one ACJ during downstroke using quasi-static analysis. For the BSCM to be stiff during downstroke, the compliant joint angle must be close to 90°.

Figure 14 shows the Pareto front of the optimization using a dynamic analysis for the BSCMs with two ACJs during the wing upstroke. This optimization converged after 145 generations. The trends observed in this plot are very similar to the trends observed in figure 13. As the deflections increase, the stresses in the designs also increase. Designs with small sweep deflection have the compliant joint angle at or close to 90°. As the compliant joint angle increases for each of the ACJs the sweep deflection of the BSCM also increases. The BSCM design shown at the bottom of this plot has significant bending displacement. This is because of the thinner compliant hinges. Hence, the thickness of the compliant hinge largely determines the upstroke stiffness of the BSCM. Bending and sweep deflections of BSCM designs with two ACJs are more than their counterparts with one ACJ (shown in figure 13). Such a comparison is shown figure 10.

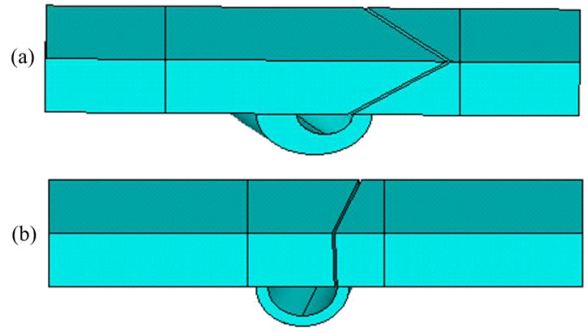

Figure 17. (a) An upstroke optimization Pareto plot member. (b) Downstroke optimization Pareto plot member. During upstroke an obtuse compliant joint angle performs well while during downstroke the compliant joint angle is preferred to be close to 90°.

This is because adding an ACJ to a BSCM decreases the stiffness of the BSCM thus making the designs more flexible.

Figure 15 shows the Pareto front of BSCM optimization with one ACJ during upstroke using quasi-static analysis. This optimization converged after 40 generations. Although the magnitudes of the bending and sweep deflections are higher when compared to BSCM optimization of one ACJ using dynamic analysis, the trends observed here are very similar to the trends observed in figure 13. From the dynamic analysis it was observed that von Mises stress and deflections are approximately linear while there was a nonlinear relation in the quasi-static case because of the nonlinear material properties and large deformation analysis. Hence these designs have larger magnitudes of bending and sweep displacements.

Figure 16 shows the Pareto front of BSCM optimization with one ACJ for downstroke using quasi-static loading conditions. This optimization converged after 60 generations. Since both sweep and bending deflections are being minimized, the Pareto front is moving towards the right bottom corner of the plot. The sweep deflection is negative because of the drag loads which cause the deflection in the negative X-direction. It was observed from this optimization that the compliant joint angle must be close to 90° if the BSCM has to be stiff during downstroke. It was also observed that these designs have larger contact angles compared to their counterparts from upstroke optimization. This is because during downstroke, the contact surfaces need to come into contact soon, if the deflections are to be minimized. These observations can be seen in the Pareto members shown in figure 17.

During the wing upstroke, the compliant joint angle is preferred to be obtuse and the contact angle acute because such a combination causes maximum bending and sweep deflection (figure 17(a)). On the other hand, during wing downstroke, for many of the BSCMs, the compliant joint angle is preferred to be close to 90° and the contact angle to be large because such a combination decreases the downstroke deflections and also causes the contact surfaces to come into contact early (figure 17(b)).

Using the design optimization procedure presented here, a designer can design a BSCM for the desired application.

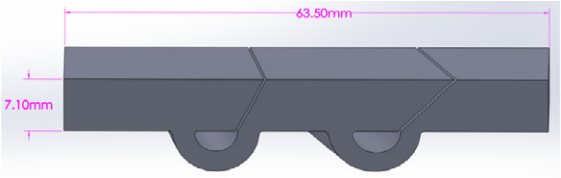

Figure 18. Solid model of an optimal bend-an-sweep compliant mechanism. The mechanism that was prototyped fits in a box with dimensions 63.5 mm × 12.7 mm × 12.7 mm, as required by the application.

Table 4. Details of an optimal bend-and-sweep compliant mechanism.

Design parameters	R_{in} (m)	R_{out} (m)	e (m)	ϕ (deg)	ϕ_{cj} (deg)
First joint (close to the tip)	0.0028	0.0056	0	62	110
Second joint (close to the root)	0.0030	0.0056	−0.0002	44	112

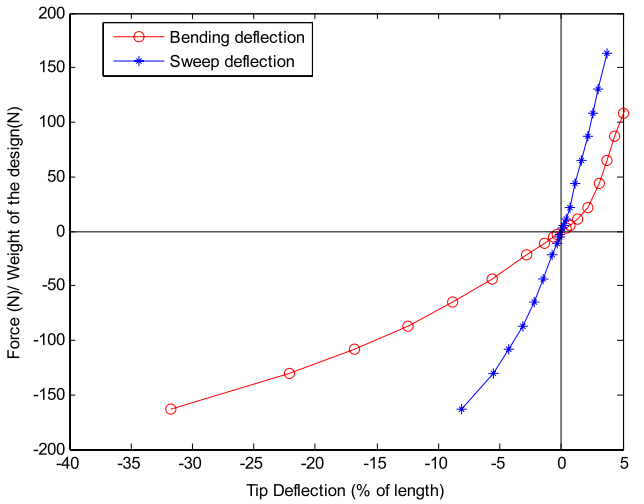

Figure 19. Stiffness plot of the optimal bend-and-sweep design. The stiffness of this mechanism is nonlinear.

Depending on the material used, the von Mises stress limit and desired deflections, a designer can select an optimal BSCM from the Pareto plot. First the importance of upstroke or downstroke deflections will have to be established. Since passive morphing during upstroke is important for the desired application, upstroke optimization results are given preference over downstroke results in this example. Based on the authors' previous experience, which includes successful bench top and flight testing with bending compliant mechanisms, the upper limit on the maximum stress under the current loading conditions was assumed to be 90% of the yield stress. Also, a maximum possible sweep deflection and a bending deflection of 8.42 mm [3] are desired. To satisfy these requirements a bend-and-sweep compliant mechanism with two ACJs will have to be chosen based on figure 10. Since the application is dynamic in nature, a member of the Pareto front (figure 14) which satisfies all the above mentioned requirements will have to be chosen. When there is more than one member of the Pareto front that satisfies the requirements, performance of all such members during downstroke will have to be considered and then an optimal design chosen. Details of one such optimal design are presented in table 4 and figure 18.

The first resonant frequency of this sample design was analyzed using ANSYS and found to be 127.55 Hz, which is well above the flapping frequency. Resonant frequencies of the other Pareto solutions are expected to be similar. The stiffness plot of this design is shown in figure 19. It can be seen from the plot that the design exhibits nonlinear stiffness in both bending and sweep directions.

5. Conclusions and future work

This paper presents a novel bend-and-sweep compliant mechanism design with nonlinear stiffness properties in two orthogonal directions. An optimization procedure was developed in order to design these BSCMs. This optimization was then applied to design a BSCM for an ornithopter application. The application required the mechanism to passively bend and sweep simultaneously.

Based on the optimization results, it was found that as the compliant joint angle becomes obtuse, the sweep deflection of the BSCM increases. The upstroke stiffness of a BSCM depends significantly on the thickness of the compliant hinge while the downstroke stiffness depends significantly on the compliant joint angle and the contact angle. Finally, adding an ACJ to a BSCM decreases its stiffness in either direction, but also adds mass to the BSCM because of the added compliant hinge, and for a particular von Mises stress value, BSCMs with more joints will have greater deflections in both bending and sweep.

Measuring the impact of the bend-and-sweep compliant mechanisms on flight performance is part of our future work. This work will include both bench top and flight testing, and will follow the protocols we developed for testing the compliant spine [4, 30]. Previous work published by the authors [4] demonstrated that the presence of a bending-only compliant spine in the leading edge spar of a flapping wing vehicle can improve its overall performance. The presence of the compliant spine was shown to reduce the power consumption by 45% and increase the mean lift produced using a test ornithopter by 16%. The compliant spine improved the vehicle performance by modifying one of the three DOF needed to perform the continuous vortex gait (CVG). It is anticipated that a bend-and-sweep compliant mechanism will implement the desired bend-and-sweep motion of the wings and achieve two, rather than one, of the DOF that are required to perform the CVG observed in birds. Thus additional lift, thrust, and power improvements are expected during steady level flight.

Acknowledgments

The authors gratefully acknowledge the support of AFOSR grants FA9550-09-1-0632 and FA9550-13-0126 under the direction of Dr David Stargel. The computational work was

supported in part through instrumentation funded by the National Science Foundation through grant OCI-0821527. The resources of the NASA Langley Research Center, Pennsylvania State University, the University of Maryland and the Morpheus Lab are also appreciated.

References

[1] Mankame N D and Ananthasuresh G K 2002 Contact aided compliant mechanisms: concept and preliminaries *Int. Design Engineering Technical Conf. and Computers and Information in Engineering Conf. (Montreal, QC)* pp 109–21 Web Portal ASME

[2] Tummala Y, Wissa A, Frecker M and Hubbard J E Jr 2010 Design of a passively morphing ornithopter wing using a novel compliant spine *Proc. Smart Materials, Adaptive Structures and Intelligent Systems Conf. (Philadelphia, PA)*

[3] Tummala Y, Wissa A, Frecker M and Hubbard J E Jr 2011 Design optimization of a compliant spine for dynamic applications *Proc. Smart Materials, Adaptive Structures and Intelligent Systems Conf. (Scottsdale, AZ)*

[4] Wissa A, Tummala Y, Hubbard J E Jr and Frecker M 2012 Passively morphing ornithopter wings using a novel compliant spine: design and testing *Smart Mater. Struct.* **21** 094028

[5] Mehta V, Frecker M and Lesieutre G 2008 Contact-aided compliant mechanisms for morphing aircraft skin *Modeling, Signal Processing, and Control for Smart Structures* (San Diego, CA: SPIE)

[6] Mehta V, Frecker M and Lesieutre G A 2012 Two-step design of multicontact-aided cellular compliant mechanisms for stress relief *Trans. ASME, J. Mech. Des.* **134** 121001

[7] Mankame N D and Ananthasuresh G K 2004 A novel compliant mechanism for converting reciprocating translation into enclosing curved paths *J. Mech. Des.* **126** 667–72

[8] Mankame N D and Ananthasuresh G K 2007 Synthesis of contact-aided compliant mechanisms for non-smooth path generation *Int. J. Numer. Methods Eng.* **69** 2564–605

[9] Reddy B V S N, Naik S V and Saxena A 2012 Systematic synthesis of large displacement contact-aided monolithic compliant mechanisms *J. Mech. Des.* **134** 011007

[10] Mehta V, Frecker M and Lesieutre G A 2009 Stress relief in contact-aided compliant cellular mechanisms *J. Mech. Des.* **131** 0910091

[11] Cirone S A, Hayes G R, Babcox B L, Frecker M, Adair J H and Lesieutre G A 2012 Design of contact-aided compliant cellular mechanisms with curved walls *J. Intell. Mater. Syst. Struct.* **23** 1773–85

[12] Halverson P A, Howell L L and Bowden A E 2008 A flexure-based bi-axial contact-aided compliant mechanism for spinal arthroplasty *Int. Design Engineering Technical Conf. & Computers and Information in Engineering Conf. (Brooklyn, NY)*

[13] Cannon J R and Howell L L 2005 A compliant contact-aided revolute joint *Mech. Mach. Theory* **40** 1273–93

[14] Bubert E A, Woods B K S, Keejoo L, Kothera C S and Wereley N M 2010 Design and fabrication of a passive 1D morphing aircraft skin *J. Intell. Mater. Syst. Struct.* **21** 1699–717

[15] Vocke R D III, Kothera C S, Woods B K S and Wereley N M 2011 Development and testing of a span-extending morphing wing *J. Intell. Mater. Syst. Struct.* **22** 879–90

[16] Barbarino S, Gandhi F and Webster S D 2011 Design of extendable chord sections for morphing helicopter rotor blades *J. Intell. Mater. Syst. Struct.* **22** 891–905

[17] Shyy W, Berg M and Ljungqvist D 1999 Flapping and flexible wings for biological and micro air vehicles *Prog. Aerosp. Sci.* **35** 455–505

[18] Wissa A, Tummala Y, Hubbard J E Jr and Frecker M 2011 Testing of novel compliant spines for passive wing morphing *Proc. Smart Materials, Adaptive Structures and Intelligent Systems Conf. (Scottsdale, AZ)*

[19] Billingsley D, Grauer J and Hubbard J E 2009 Testing of a passively morphing ornithopter wing *AIAA AUU (Seattle, WA)*

[20] Brown R H J 1953 The flight of birds: wing function in relation to flight speed *J. Exp. Biol.* **30** 90–103

[21] Banerjee J R and Su H 2006 Free transverse and lateral vibration of beams with torsional coupling *J. Aero. Eng.* **19** 13–20

[22] Zhou A, Qu B-Y, Li H, Zhao S-Z, Suganthan P N and Zhang Q 2011 Multiobjective evolutionary algorithms: a survey of the state of the art *Swarm Evol. Comput.* **1** 32–49

[23] Deb K, Pratap A, Agarwal S and Meyarivan T 2002 A fast and elitist multiobjective genetic algorithm: NSGA-II *IEEE Trans. Evol. Comput.* **6** 182–97

[24] Deb K 2001 *Multi-Objective Optimization Using Evolutionary Algorithms* (Chichester: Wiley)

[25] Deb K and Jain S 2002 Running performance metrics for evolutionary multi-objective optimization *Proc. 4th Asia-Pacific Conf. on Simulated Evolution and Learning (Singapore)*

[26] Kollat J B and Reed P M 2006 Comparing state-of-the-art evolutionary multi-objective algorithms for long-term groundwater monitoring design *Adv. Water Resour.* **29** 792–807

[27] Tobalske B W 2000 Biomechanics and physiology of gait selection in flying birds *Physiol. Biochem. Zool.* **73** 736–50

[28] Dupont 2011 http://plastics.dupont.com/plastics/pdflit/americas/delrin/230323c.pdf

[29] Olympio K R 2006 Design of a passive flexible skin for morphing aircraft structures *MS Thesis* The Pennsylvania State University

[30] Wissa A, Guerreiro N, Grauer J, Hubbard J E Jr, Altenbuchner C, Tummala Y, Frecker M and Roberts R 2013 Flight testing of novel compliant spines for passive wing morphing on ornithopters *21st AIAA/ASME/AHS Adaptive Structures Conf. (Boston, MA)*